THE JOURNAL OF PHYSICAL CHEMISTRY C

Article

pubs.acs.org/JPCC

Surface on Surface. Survey of the Monolayer Gold−Graphene Interaction from Au_{12} and PAH via Relativistic DFT Calculations

Alvaro Muñoz-Castro,*[,†] Tatiana Gomez,[†] Desmond MacLeod Carey,[†] Sebastian Miranda-Rojas,[‡] Fernando Mendizabal,[§] Jose H. Zagal,[∥] and Ramiro Arratia-Perez[‡]

[†]Grupo de Química Inorgánica y Materiales Moleculares, Universidad Autonoma de Chile, El Llano Subercaseaux 2801, Santiago, Chile

[‡]Departamento de Ciencias Químicas, Relativistic Molecular Physics (ReMoPh) Group, Universidad Andres Bello, Republica 275, Santiago, Chile

[§]Departamento de Química, Facultad de Ciencias, Universidad de Chile, P.O. Box 653, Las Palmeras 3425, Ñuñoa, Santiago, Chile

[∥]Departamento de Química de los Materiales, Facultad de Química y Biología, Universidad de Santiago de Chile, Av. Libertador B. O'Higgins 3363, Casilla 40, Correo 33, Santiago, Chile

Supporting Information

ABSTRACT: Gold−graphene interaction at the interface is evaluated through different polyaromatic hydrocarbons (PAH), accounted by C_6H_6, $C_{24}H_{12}$, $C_{54}H_{16}$, and $C_{96}H_{18}$, focusing into different energetic terms related to the overall interaction. Our results characterize the neutral gold−PAH interaction nature with 45% of dispersion character, 35% of electrostatic, and 20% of covalent character, suggesting that moderate van der Waals character is mostly involved in the interaction, which increases according to the size of the respective PAH. The resulting surface charge distribution in the graphene model is a relevant parameter to take into account, since the ability of the surface charge to be reorganized over the polycyclic structure in both contact and surrounding regions is important in order to evaluate interactions and different interacting conformations. Our results suggest that for a Au_{12} contact surface of radius 4.13 Å, the covalent, electrostatic and dispersion character of the interaction are effectively accounted in a graphene surface of about 6.18 Å, as given by circumcoronene, depicting a critical size where the overall interaction character can be accounted.

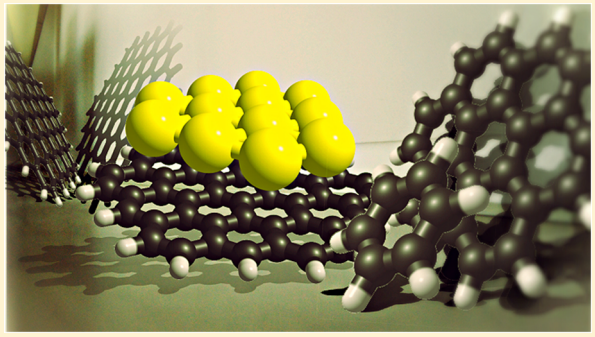

INTRODUCTION

Two-dimensional materials have attracted great attention from both experimental and theoretical scientists in recent years due to their large surface area and novel electronic, thermal, mechanical, and chemical properties.[1−5] Especially graphene nanosheets (GNS) combine unique structures and excellent mechanical and electrical properties with atomic thickness, which makes them one of the most suitable candidates for future nanoelectronics[4] and hold great promise for widespread applications in energy storage,[2] supercapacitors,[3,5] sensors,[6] and nanocomposites.[7−11]

Taking advantage of chemical vapor deposition (CVD) methods, few layers of graphene can be grown resulting in high optical transparency, flexible and low sheet resistance devices, which are ready to transfer to other substrates.[12,13] Offering large-scale graphene electrodes composed predominantly of mono- and bilayers,[12] supporting a potential replacement for silicon electronics. Moreover, inclusion of graphene in hybrid devices has shown the enhancement of some relevant properties.[14] It has been shown that magnetite−graphene composites are more stable to ambient conditions than magnetite, with enhanced binding capacity to As(III) and As(IV), being useful for practical arsenic separation from polluted water.[15]

DNA sequencing is another promising application involving graphene layers, which has been evaluated theoretically by using state-of-art transport simulation showing a feasible current measurement through $\pi-\pi$ interaction as DNA passes along from an appropriate device.[16] This points out the main role of noncovalent interactions toward the realization of versatile and reusable devices. Graphene is also an ideal material for novel spectroscopy methods based on both bias and gate voltages, leading to characterization tools capable of describing molecular fingerprints with atomic resolution.[17]

The interaction with different molecules, clusters, or even single atoms induces deep changes in graphene properties which have been investigated in detail.[3−6] In this regard, further development of graphene-based devices requires the presence

Received: December 23, 2015
Revised: March 21, 2016
Published: March 24, 2016

DOI: 10.1021/acs.jpcc.5b12580
J. Phys. Chem. C 2016, 120, 7358−7364

of graphene−metal contacts[7−11] leading to novel changes in its properties such as charge transfer[8,9] contact resistance and electron transport.[10,11] Noticeable progress has been made in the biosensor field, where reduced graphene oxide (rGO)/gold nanocomposites substantially improve the glucose sensor capabilities of chitosan/graphene oxide (GOx) over a glassy carbon electrode (GCE).[18] Also, other metal/graphene composites have shown amperometric response to relevant biomolecules[19] paving the way to promising biosensing applications which have been reviewed recently.[20,21]

Interestingly, gold/graphene, among other noble metal-based composites,[22] exhibits remarkable properties for application as a new generation of electrochemical active devices and biosensors for enzyme detection.[23] The possibility of graphene n-type doping has also been explored by functionalized gold particles with promising applications in graphene-based electronic devices,[24] denoting the great potential of gold/graphene composites. Another interesting advantage of the inclusion of gold aggregates into graphene is the enhanced binding energy observed for defects leading to the growth of larger sizes, being a clever strategy for characterization via scanning tunneling microscopy (STM) among other techniques.[25] In this regard, we are also interested in Au(111) surfaces as they provide very important substrates for anchoring molecules with catalytic activity for ET reactions such as O_2 reduction.[26−29] We are currently interested in producing hybrid electrodes with gold and graphene[30] for electrocatalytic studies.

Moreover, interaction between neutral monolayer models, offers an interesting scenario to gain a better understanding of the noncovalent phenomenon occurring at the gold−graphene interface. Two-dimensional arrangements of gold atoms are of importance because they offer reliable models to gain a better understanding of the interactions between substrates and coinage-metal surfaces in heterogeneous catalysis and metal surface reactions.[31−37] For our study, an appropriate molecular model for Au(111) surface toward the understanding of weak surface−surface interactions should deliver a few important features: (i) closed-shell electronic structure, (ii) symmetrically compatible with a graphene surface, and (iii) neutral charge state. The latter point is needed in order to avoid an artificial enhancement of the interaction ionic character due to charged species. A required structural conformation should involve at least a C_3 symmetry operation, matching with the C_3 rotation axis of a honeycomb lattice for a regular graphene sheet.

In this sense two potential candidates are given by Au_{10} and Au_{12} which both can display D_{3h} conformation. From the conformational analysis of Kim and co-workers, D_{3h}-Au_{10} is located 49.6 kcal/mol (2.15 eV) above the minima D_{2h} conformation, displaying an open-shell triplet ground state.[38] Au_{12} exhibits a minima D_{3h} conformation, which is located 6.7 kcal/mol above the next isomer according to Kuz'menko's group.[39] The 12 valence electrons of the neutral cluster lead to a closed-shell electronic structure, which can be understood in terms of the planar superatomic model according to a $1s^21p^41d^42s^2$ electronic configuration.[40] In addition, the D_{3h} conformation is also obtained for the monoanionic species from the data of negatively charged gold clusters.[37] Thus, D_{3h}-Au_{12} is a prototypical model which is able to reproduce the Au(111) surface of bulk gold with small distortions,[39] being a prototypical model to study interactions at the graphene/metal interface.

As part of our current research, herein we report a relativistic computational study of the several monolayer−monolayer interaction models of gold−graphene nanocomposites, in order to address the stability, electronic structure modifications, and light absorption capabilities of the single-layer interface. Our model considers the Au_{12} cluster adsorbed on several models of graphene sheets, given by polycyclic aromatic hydrocarbon (PAH) molecules of increasing size,[41−45] going from benzene (C_6H_6), coronene ($C_{24}H_{12}$), and circumcoronene ($C_{54}H_{18}$) to circumcircumcoronene ($C_{96}H_{18}$) in order to study the size effects of the hydrocarbon surface into the strength and nature of such interactions.

COMPUTATIONAL DETAILS

Relativistic density functional theory calculations[46] were carried out by using the ADF code,[47] incorporating scalar corrections via the ZORA Hamiltonian.[48,49] We employed the triple-ζ Slater basis set, plus two polarization functions (STO-TZ2P) for valence electrons, within the generalized gradient approximation (GGA) according to the Perdew−Burke−Ernzerhof (PBE) nonlocal exchange-correlation functional.[50,51] We used this set because of its improved performance on long-range interactions and relatively low computational cost for larger molecules.[52,53] The frozen core approximation was applied to the $[1s^2\text{-}4f^{14}]$ core for Au, and $[1s^2]$ for C, leaving the remaining electrons to be treated variationally. Geometry optimizations were performed without any symmetry restraint, via the analytical energy gradient method implemented by Verluis and Ziegler.[54] In order to include dispersion corrections, the semiempirical DFT-D3 method of Grimme was employed,[55] depicted as PBE-D3. For comparison, Hartree−Fock (HF), second-order Møller−Plesset Perturbation (MP2), and spin-component-scaled Møller−Plesset theory (SCS-MP2) calculations were carried out. The latter calculations were done using Gaussian 09.[56] For Au atoms, we used the scalar relativistic Stuttgart pseudopotentials (PP): 19 valence-electron (VE) for Au.[57] The calculations have been performed using the set VDZP with two f-type (2f) polarization functions (α_f = 0.20, 1.19).[58] It has already been shown that is necessary to use functions with diffusion and polarization to correctly describe the weak dispersion interactions.[59−62] Also, the C atom was treated through PPs, using double-ζ basis sets with the addition of one d-type polarization function.[63] For the H atom, a double-ζ basis set plus one p-type polarization function was used.[64]

RESULTS AND DISCUSSION

The gold−graphene interface was evaluated via the planar Au_{12} cluster and different polycyclic aromatic hydrocarbon (PAH) molecules. Two main conformations of the layer interaction can be drawn considering the spatial disposition of the gold cluster absorbed into the PAH surfaces, namely, top (Au−C), where gold atoms located mainly over carbon sites, and bridge (Au-CC) between C−C bonds. Schematic representations of the studied systems are depicted in Figure 1, where gold−surface distances range from 3.370 to 3.479 Å at the equilibrium structures, displaying small differences between each conformation (Tables 1 and 2). Slight structural variations upon formation of the Au_{12}−PAH pair are accounted by the deformation or preparation energy (ΔE_{prep}), which amounts to an average of 1.15 kcal/mol for Au_{12} and of 0.30 kcal/mol for the different PAH. This term is in line with the weak nature of the interaction. In the case given by circumcoronene ($C_{54}H_{18}$) and circumcircumcoronene ($C_{96}H_{24}$), the inclusion of Au_{12}

DOI: 10.1021/acs.jpcc.5b12580
J. Phys. Chem. C 2016, 120, 7358−7364

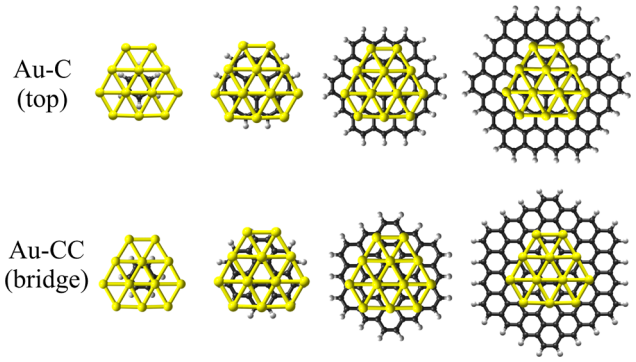

Figure 1. Schematic representation of the studied systems.

leads to small distortions in the hydrocarbon surface resulting in a bowl-shaped deviation of 0.144 and 0.318 Å of concavity, respectively, depicting the flexibility of larger PAH for minimizing steric repulsion. In addition, small structural modifications are observed for Au_{12}, where the main feature is given by a related bowl-shaped distortion, which is more pronounced in the Au−C conformation, and decreases toward PAH with larger surfaces.

The resulting Au_{12}−PAH interaction leads to an energetically favorable situation, as given by the interaction energy (ΔE_{int}) (Tables 1 and 2). Such values increase from −15.69 to −56.74 kcal/mol, as the number of fused aromatic rings involved increase according to the respective PAH. Interestingly, the stabilizing energy trend converges around to −50 kcal/mol for the larger counterparts. By comparing both Au−C and Au−CC conformations, the latter situation is slightly more favorable depicting the preference of Au_{12} cluster to allocate a gold atom over the C−C bonds (bridge position).

It is well-known that calculations of the interaction energy in noncovalently bound systems by using MP2 approximation overestimate attractive interactions;[65−67] however, it gives a good indication of their existence. A more precise post-Hartree−Fock treatment is given by CCSD(T), increasing considerably the computational cost. Moreover, the spin-component-scaled (SCS) MP2 method has been shown to produce results comparable to CCSD(T) at a relatively low computational demand. Thus, SCS-MP2 is considered an accurate and efficient tool for incorporating electronic correlation to the study of large systems. On the other hand, at the Hartree−Fock level lower interaction energies are obtained. This shows that when using methods that do not include dispersion effects, the attraction between Au_{12} and PAH decreases, denoting the importance of their inclusion.

In the literature, the smallest theoretical model for Au−π interaction is given by the Au-ethylene system.[66] It was found that the interaction between Au and ethylene (on bond double bond) are due to a correlation electronic effect, strengthened by relativistic contributions. The interaction energy shows a strong oscillation toward higher levels of electronic correlation, i.e., going from MP2 to MP3, MP4, CCSD, and CCSD(T) models. Such values vary from 5.82 kcal/mol at MP2 level to 3.13 kcal/mol at CCSD(T), denoting the overstabilization obtained from MP2 calculations in comparison to higher levels of electronic correlation within Hartree−Fock. For our systems, the respective values obtained at MP2 and SCS-MP2 are in line with the results obtained at the PBE-D3 level; thus, hereafter we focus our analysis on the results provided by TZ2P/PBE-D3 calculations.

In order to have a better understanding of the nature of the interaction energy (E_{int}), we performed the energy decomposition analysis (EDA) within the Morokuma−Ziegler scheme,[68,69] leading to different chemically meaningful contributing terms according to

$$\Delta E_{int} = \Delta E_{orb} + \Delta E_{elstat} + \Delta E_{disp} + \Delta E_{Pauli}$$

Here, the stabilizing ΔE_{elstat} term refers to the electrostatic character of the interaction, which is obtained by considering each defined fragment (namely, A and B) in its unperturbed (frozen) electron density as isolated species ($\Psi_A\Psi_B$). Next, the repulsive ΔE_{Pauli} term accounts for the four-electron two-orbital interactions between occupied orbitals, which is calculated from the energy change in the process of antisymmetrization and renormalization of the overlapped fragment densities ($\Psi_0 = N\hat{A}\{\Psi_A\Psi_B\}$). Finally, the stabilizing ΔE_{orb} term obtained when the densities of the constituent fragments relax into the final molecular orbitals (Ψ_{AB}) accounts for the covalent character of the interaction. In addition, the pairwise correction of Grimme (DFT-D3) allows us to evaluate the dispersion interaction (ΔE_{disp}) related to London forces. To overcome basis set superposition error (BSSE), the counterpoise method[64] was employed, which amounts to <2 kcal/mol.

The relative contribution of the stabilizing terms given by ΔE_{orb}, ΔE_{elstat}, and ΔE_{disp}, accounts for the overall character of the interaction. In all the series, the ΔE_{disp} term is the main term, contributing in a larger amount accounting for about of 45% of the stabilizing energy, in agreement with the van der Waals character of the Au_{12}−PAH interaction. The electrostatic nature of the interaction, given by ΔE_{elstat}, accounts for the 35%, where the remaining contribution is of covalent character (20%).

The repulsive Pauli term increases according to the size of the respective PAH, depicting similar values for the larger systems, namely, $C_{54}H_{18}$ and $C_{96}H_{24}$, suggesting that the overall repulsive terms for a gold surface of the size of Au_{12} can effectively be accounted by the former PAH.

For the different structures, ΔE_{elstat} increases from −13.71 to −40.17 kcal/mol, which converge at circumcoranene, as denoted by the similar value between such systems and the circumcircumcoranene counterpart. Also, this stabilizing term is

Table 1. Au_{12}−PAH Distance (Å) and Energy Decomposition Analysis of the Studied Complexes in Au−C Conformation

PAH	C_6H_6		$C_{24}H_{12}$		$C_{54}H_{18}$		$C_{96}H_{24}$	
Au_{12}−PAH	3.369		3.397		3.446		3.454	
ΔE_{pauli}	22.88		40.81		55.24		57.96	
ΔE_{elect}	−14.42	37.4%	−26.41	34.8%	−37.24	35.4%	−38.31	33.8%
ΔE_{orb}	−8.79	22.8%	−16.73	22.1%	−19	18.1%	−20.63	18.2%
ΔE_{disp}	−15.36	39.8%	−32.7	43.1%	−48.9	46.5%	−54.57	48.1%
ΔE_{int}	−15.69		−35.03		−49.9		−55.55	

DOI: 10.1021/acs.jpcc.5b12580
J. Phys. Chem. C 2016, 120, 7358−7364

Table 2. Au_{12}−PAH Distance (Å) and Energy Decomposition Analysis of the Studied Complexes in Au−CC Conformation

	C_6H_6		$C_{24}H_{12}$		$C_{54}H_{18}$		$C_{96}H_{24}$	
Au_{12}−PAH	3.370		3.363		3.456		3.479	
ΔE_{pauli}	20.54		56.02		60.38		60.73	
ΔE_{elect}	−13.71	37.7%	−34.77	38.0%	−40.17	36.1%	−40.04	34.1%
ΔE_{orb}	−8.01	22.0%	−20.82	22.8%	−20.68	18.6%	−21.64	18.4%
ΔE_{disp}	−14.64	40.3%	−35.87	39.2%	−50.36	45.3%	−55.79	47.5%
ΔE_{int}	−15.82		−35.44		−50.83		−56.74	

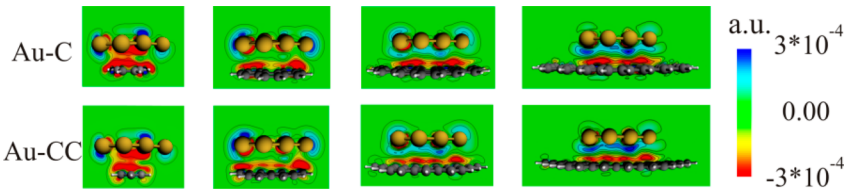

Figure 2. Charge density difference maps.

the most dependent in relation to the given conformation, namely, Au−C or Au−CC, where such differences decrease according to the PAH size.

By using difference charge-density distribution maps, the spatial distribution of charge density fluctuations can be accounted, involving mostly a π-orbital character. Here, the contour-plot bisecting the Au_{12} cluster (Figure 2) exhibits a main charge depletion region in such structure, and the respective charge accumulation compromising mainly the π-orbitals of the respective PAH. Thus, the covalent character in the interface interaction can be ascribed to the small gold→PAH charge donation which occurs solely in the interacting face of the polyaromatic structure. Through the series, the ΔE_{orb} term increases from −8.01 to −21.64 kcal/mol being the less affected term according to the PAH size, as can be seen from the smaller variation found between circumcoranene and circumcircumcoranene. This fact suggests that at such size it is possible to account for mostly the overall covalent character, similarly to the behavior of the interaction electrostatic character.

By comparing both Au−C and Au−CC conformations, the variation of the ΔE_{orb} term is larger in the coronene case, decreasing toward larger counterparts. Interestingly, for the smaller case, namely, Au_{12}−C_6H_6, such a difference is less than 1 kcal/mol, suggesting that the influence of the conformation over this stabilizing term is relevant in medium-sized PAH. The spatial charge distribution over the PAH surface was evaluated by using the potential energy surfaces (Figure 3). Comparing the respective potential energy surface for the isolated PAH, some size-dependent features are found. In the smaller aromatic system (C_6H_6), a small variation between the surface charge distributions in both conformations (Au−C and Au−CC) is observed, which agrees with the slight variation of the stabilizing ΔE_{orb} and ΔE_{elstat} terms. In contrast, the next structure ($C_{24}H_{12}$) exhibits a large difference in such charge distribution between both conformations, which is in line with the largest difference between such stabilizing terms amounting to about −4.0 and −8.0 kcal/mol, respectively. In $C_{54}H_{18}$, both conformations lead to similar charge distribution, depicting some differences due to the confinement given by the size of such PAH, which produce smaller differences in such stabilizing terms, in comparison to coranonene, amounting to −1.0 and −3.0 kcal/mol, respectively. For $C_{96}H_{24}$, a larger structure allows more flexibility to reorganize the surface charge upon

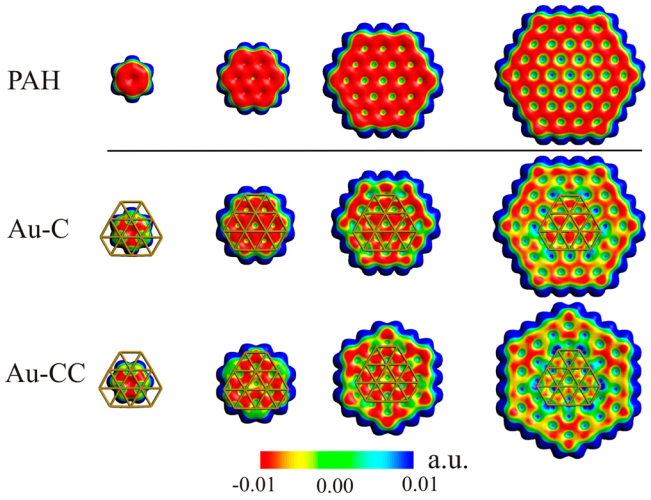

Figure 3. Potential energy surface at the PAH surface, depicting the variation upon inclusion of the Au_{12} cluster.

inclusion of Au_{12}, which is denoted by the differences of about −1.0 and −2.0 kcal/mol, in ΔE_{orb} and ΔE_{elstat} terms. The resulting surface charge distribution in both conformations is similar from coronene to circumcircumcoronene, where the differences are given by the rings located outside of the interacting region. In this regard, the smaller variation possibilities for benzene lead to smaller energetic terms. Hence, the ability of the surface charge to be reorganized over the polycyclic structure in both contact and surrounding regions is a relevant feature to be taken into account in order to evaluate interactions and different interacting conformations.

Finally, the relevant ΔE_{disp} term increases from −14.64 to −55.79 kcal/mol along the series. From benzene to coronene, a stabilization of about −20.0 kcal/mol is observed due to the increase in the contact surface of PAH. Interestingly, from the latter to circumcoronene, a subsequent stabilization of about −15.0 kcal/mol is depicted, reaching an extra stabilization of about −5.0 kcal/mol for the next polyaromatic structure. This result suggests that from the size of circumcoronene it is possible to account for mostly of the overall van der Waals forces related to the inclusion of the Au_{12} cluster.

In order to evaluate the spatial distribution of the weak forces accounted by the ΔE_{disp} term, we employed the noncovalent interaction index (NCI)[70−72] for the studied series (Figure 5).

DOI: 10.1021/acs.jpcc.5b12580
J. Phys. Chem. C 2016, 120, 7358−7364

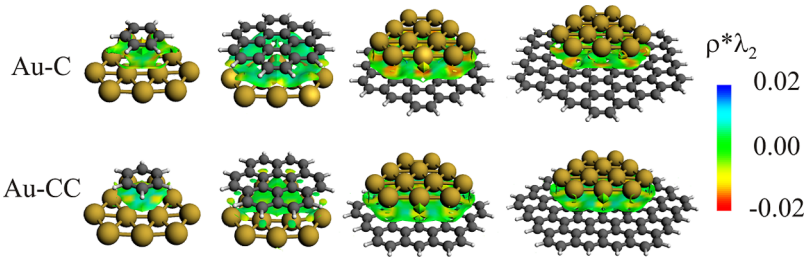

Figure 4. Noncovalent index analysis.

The NCI index offers a suitable description of noncovalent interactions based on the reduced density gradient ($s(\rho)$) at low-density regions ($\rho(r) < 0.06$ a.u.). The $s(\rho)$ quantity is employed to denote a nonhomogenenous or electron distribution and is given by

$$s = \frac{1}{2(3\pi^2)^{1/3}} \frac{\nabla\rho}{p^{4/3}}$$

$s(\rho)$ exhibits small values in regions where noncovalent interactions are located, where its stabilizing or destabilizing nature can be addressed by the second eigenvalue of the electron density Hessian (λ_2). This accounts for the accumulation (attractive) or depletion (repulsive) of density in the plane perpendicular to the interaction. Thus, the product between $\rho(r)$ and the sign of λ_2 has been proposed as a useful descriptor denoting: stabilizing ($\lambda_2 < 0$), weak ($\lambda_2 \approx 0$) or repulsive interactions ($\lambda_2 > 0$)[44−46], where ρ^* sign (λ_2) ranges from negative to positive values unraveling the nature of the noncovalent interaction.

Figure 4 illustrates the regions where noncovalent interactions are relevant, where the ρ^* sign(λ_2) is close to zero. This allows one to account for van der Waals forces between PAH and Au_{12}. In addition, some weak hydrogen−Au_{12} interaction can be observed for coronene and benzene counterparts. In the Au−C conformation, stabilizing regions are observed locally in the Au−C contact. Moreover, for Au−CC conformations a related stabilizing region is observed through the Au−CC contact, depicting a slightly more stabilizing situation. Interestingly, the NCI plots can be related to the almost constant increase of ΔE_{disp} up to $C_{54}H_{18}$ as discussed above, because such structure exhibits a surface size appropriate for recovering most of the contact regions related to van der Waals forces. From $C_{54}H_{18}$ to $C_{96}H_{24}$, a similar NCI region can be observed, which is in line with the small variation of ΔE_{disp} of about −5.0 kcal/mol.

The results discussed above suggest that for a Au_{12} contact surface, of radius 4.13 Å, the covalent, electrostatic, and dispersion character, and Pauli repulsion term of the interaction are effectively accounted in a graphene surface of about 6.18 Å, as given by circumcoronene. This observation allows us to suggest a simple rule for gold−graphene interaction, where the radius of the interacting graphene face should be of 50% larger than the gold-interacting face. Such a region accounts for the main variation in current measurements for incoming substrates, which is of relevance for sensor capabilities based on electronic transmission.[20] Hence, further studies will focus on the changes in the interlayer noncovalent interaction in electron attachment/detachment situations.

Due to the increasing size of the PAH surface, the frontier electronic structure exhibits a π-orbital character. The schematic electronic structure for the systems including different PAH is depicted in Figure 5. All the systems exhibit a low energy $\pi \rightarrow Au_{12}$ allowed electronic transition, where the

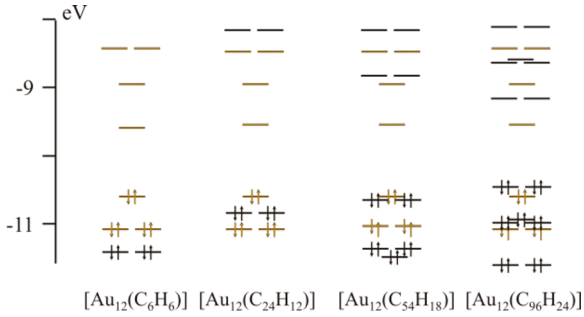

Figure 5. Schematic representation of the electronic structure of the studied systems. Code: Yellow, denotes Au_{12} electronic levels; Black, denotes π-PAH levels.

dipole-moment change is contained in the *xy*-plane. Our results show that such transition decreases in energy from 1.84 eV for C_6H_6 to 0.90 eV for $C_{96}H_{24}$; due to the increase in size of the respective PAH, the dipole moment change decreases, leading to lesser allowed transition. Thus, it is not expected to be observable in larger systems. The next relevant $\pi \rightarrow Au_{12}$ transition is located at 2.96 eV for benzene, resulting from a *z*-axis polarization, which, similarly to that depicted previously, decreases in energy and becomes less allowed. Thus, this low-energy transition can be used to evaluate the size of the interacting graphene surface. For all the systems, intra-Au_{12} transitions are observed at about 1.7, 2.5, and 2.8 eV, whereas relevant intra-PAH transitions are observed starting from circumcoronene at 2.9 and 1.7 eV for circumcircumcoronene.

4. CONCLUSIONS

The evaluation of the gold−graphene interaction given by different hydrogenated graphene models, accounted by C_6H_6, $C_{24}H_{12}$, $C_{54}H_{16}$, and $C_{96}H_{18}$, allows detailed study of the different energetic terms related to the overall interaction. By comparing the different stabilizing terms relevant to the neutral gold−PAH pair formation, the interaction exhibits about 45% dispersion character, 35% electrostatic, and 20% covalent character, suggesting that moderate van der Waals character is mostly involved in the interaction, which increases according to the size of the respective PAH. The resulting surface charge distribution in the graphene model is a relevant parameter to take into account. The ability of the surface charge to be reorganized over the polycyclic structure in both contact and surrounding regions is important in order to evaluate interactions and different interacting conformations.

Our results suggest that for a Au_{12} contact surface, of radius 4.13 Å, the covalent, electrostatic, and dispersion character of

DOI: 10.1021/acs.jpcc.5b12580
J. Phys. Chem. C 2016, 120, 7358−7364

the interaction are effectively accounted in a graphene surface of about 6.18 Å, as given by circumcoronene. This observation allows drawing a simple rule for gold−graphene interaction, where the radius of the graphene surface should be 50% larger than the respective metallic interacting face. Further work toward a deeper understanding of gold/graphene defect interactions is in progress.

■ ASSOCIATED CONTENT

Supporting Information

The Supporting Information is available free of charge on the ACS Publications website at DOI: 10.1021/acs.jpcc.5b12580.

Graphene−PAH interaction energy at different levels of theory (PDF)

■ AUTHOR INFORMATION

Corresponding Author

*E-mail: alvaro.munoz@uautonoma.cl.

Notes

The authors declare no competing financial interest.

■ ACKNOWLEDGMENTS

The authors thank the MILLENNIUM PROJECT RC120001 for support our collaborative efforts.

■ REFERENCES

(1) Novoselov, K. S.; Geim, A. K.; Morozov, S. V.; Jiang, D.; Zhang, Y.; Dubonos, S. V.; Grigorieva, I. V.; Firsov, A. A. Electric Field Effect in Atomically Thin Carbon Films. *Science* **2004**, *306* (5696), 666−669.

(2) Geim, A. K.; Novoselov, K. S. The Rise of Graphene. *Nat. Mater.* **2007**, *6* (3), 183−191.

(3) Ruoff, R. Graphene: Calling All Chemists. *Nat. Nanotechnol.* **2008**, *3* (1), 10−11.

(4) Stankovich, S.; Dikin, D. A.; Dommett, G. H. B.; Kohlhaas, K. M.; Zimney, E. J.; Stach, E. A.; Piner, R. D.; Nguyen, S. T.; Ruoff, R. S. Graphene-Based Composite Materials. *Nature* **2006**, *442* (7100), 282−286.

(5) Lu, X.; Yu, M.; Huang, H.; Ruoff, R. S. Tailoring Graphite with the Goal of Achieving Single Sheets. *Nanotechnology* **1999**, *10* (3), 269.

(6) Schedin, F.; et al. Detection of Individual Gas Molecules Adsorbed on Graphene. *Nat. Mater.* **2007**, *6* (9), 652.

(7) Wintterlin, J.; Bocquet, M.-L. Graphene on Metal Surfaces. *Surf. Sci.* **2009**, *603* (10−12), 1841−1852.

(8) Gierz, I.; Riedl, C.; Starke, U.; Ast, C. R.; Kern, K. Atomic Hole Doping of Graphene. *Nano Lett.* **2008**, *8* (12), 4603−4607.

(9) Giovannetti, G.; Khomyakov, P. A.; Brocks, G.; Karpan, V. M.; van den Brink, J.; Kelly, P. J. Doping Graphene with Metal Contacts. *Phys. Rev. Lett.* **2008**, *101* (2), 26803.

(10) Barraza-Lopez, S.; Vanević, M.; Kindermann, M.; Chou, M. Y. Effects of Metallic Contacts on Electron Transport through Graphene. *Phys. Rev. Lett.* **2010**, *104* (7), 76807.

(11) Lee, E. J. H.; Balasubramanian, K.; Weitz, R. T.; Burghard, M.; Kern, K. Contact and Edge Effects in Graphene Devices. *Nat. Nanotechnol.* **2008**, *3* (8), 486−490.

(12) Kim, K. S.; Zhao, Y.; Jang, H.; Lee, S. Y.; Kim, J. M.; Kim, K. S.; Ahn, J.-H.; Kim, P.; Choi, J.-Y.; Hong, B. H. Large-Scale Pattern Growth of Graphene Films for Stretchable Transparent Electrodes. *Nature* **2009**, *457* (7230), 706−710.

(13) Jeon, C.; Hwang, H.-N.; Lee, W.-G.; Jung, Y. G.; Kim, K. S.; Park, C.-Y.; Hwang, C.-C. Rotated Domains in Chemical Vapor Deposition-Grown Monolayer Graphene on Cu(111): An Angle-Resolved Photoemission Study. *Nanoscale* **2013**, *5* (17), 8210−8214.

(14) Kemp, K. C.; Seema, H.; Saleh, M.; Le, N. H.; Mahesh, K.; Chandra, V.; Kim, K. S. Environmental Applications Using Graphene Composites: Water Remediation and Gas Adsorption. *Nanoscale* **2013**, *5* (8), 3149−3171.

(15) Chandra, V.; Park, J.; Chun, Y.; Lee, J. W.; Hwang, I.-C.; Kim, K. S. Water-Dispersible Magnetite-Reduced Graphene Oxide Composites for Arsenic Removal. *ACS Nano* **2010**, *4* (7), 3979−3986.

(16) Min, S. K.; Kim, W. Y.; Cho, Y.; Kim, K. S. Fast DNA Sequencing with a Graphene-Based Nanochannel Device. *Nat. Nanotechnol.* **2011**, *6* (3), 162−165.

(17) Rajan, A. C.; Rezapour, M. R.; Yun, J.; Cho, Y.; Cho, W. J.; Min, S. K.; Lee, G.; Kim, K. S. Two Dimensional Molecular Electronics Spectroscopy for Molecular Fingerprinting, DNA Sequencing, and Cancerous DNA Recognition. *ACS Nano* **2014**, *8* (2), 1827−1833.

(18) Bai, X.; Shiu, K.-K. Investigation of the Optimal Weight Contents of Reduced Graphene Oxide−gold Nanoparticles Composites and Theirs Application in Electrochemical Biosensors. *J. Electroanal. Chem.* **2014**, *720−721*, 84−91.

(19) Wang, L.; Lu, X.; Ye, Y.; Sun, L.; Song, Y. Nickel-Cobalt Nanostructures Coated Reduced Graphene Oxide Nanocomposite Electrode for Nonenzymatic Glucose Biosensing. *Electrochim. Acta* **2013**, *114*, 484−493.

(20) Tiwari, J. N.; Vij, V.; Kemp, K. C.; Kim, K. S. Engineered Carbon-Nanomaterial-Based Electrochemical Sensors for Biomolecules. *ACS Nano* **2016**, *10* (1), 46−80.

(21) Tiwari, J. N.; Kemp, K. C.; Nath, K.; Tiwari, R. N.; Nam, H.-G.; Kim, K. S. Interconnected Pt-Nanodendrite/DNA/Reduced-Graphene-Oxide Hybrid Showing Remarkable Oxygen Reduction Activity and Stability. *ACS Nano* **2013**, *7* (10), 9223−9231.

(22) Tiwari, J. N.; Nath, K.; Kumar, S.; Tiwari, R. N.; Kemp, K. C.; Le, N. H.; Youn, D. H.; Lee, J. S.; Kim, K. S. Stable Platinum Nanoclusters on Genomic DNA−graphene Oxide with a High Oxygen Reduction Reaction Activity. *Nat. Commun.* **2013**, *4*, 3221.

(23) Myung, S.; Yin, P. T.; Kim, C.; Park, J.; Solanki, A.; Reyes, P. I.; Lu, Y.; Kim, K. S.; Lee, K.-B. Label-Free Polypeptide-Based Enzyme Detection Using a Graphene-Nanoparticle Hybrid Sensor. *Adv. Mater.* **2012**, *24* (45), 6081−6087.

(24) Huh, S.; Park, J.; Kim, K. S.; Hong, B. H.; Kim, S. Bin. Selective N-Type Doping of Graphene by Photo-Patterned Gold Nanoparticles. *ACS Nano* **2011**, *5* (5), 3639−3644.

(25) Yu, S. U.; Park, B.; Cho, Y.; Hyun, S.; Kim, J. K.; Kim, K. S. Simultaneous Visualization of Graphene Grain Boundaries and Wrinkles with Structural Information by Gold Deposition. *ACS Nano* **2014**, *8* (8), 8662−8668.

(26) Nyokong, T.; Bedioui, F. Self-Assembled Monolayers and Electropolymerized Thin Films of Phthalocyanines as Molecular Materials for Electroanalysis. *J. Porphyrins Phthalocyanines* **2006**, *10* (09), 1101−1115.

(27) Ponce, I.; Silva, J. F.; Oñate, R.; Rezende, M. C.; Páez, M. A.; Pavez, J.; Zagal, J. H. Enhanced Catalytic Activity of Fe Phthalocyanines Linked to Au (111) via Conjugated Self-Assembled Monolayers of Aromatic Thiols for O 2 Reduction. *Electrochem. Commun.* **2011**, *13* (11), 1182−1185.

(28) Ponce, I.; Silva, J. F.; Oñate, R.; Miranda-Rojas, S.; Muñoz-Castro, A.; Arratia-Pérez, R.; Mendizabal, F.; Zagal, J. H. Theoretical and Experimental Study of Bonding and Optical Properties of Self-Assembly Metallophthalocyanines Complexes on a Gold Surface. A Survey of the Substrate−Surface Interaction. *J. Phys. Chem. C* **2011**, *115* (47), 23512−23518.

(29) Ponce, I.; Silva, J. F.; Oñate, R.; Rezende, M. C.; Paez, M. A.; Zagal, J. H.; Pavez, J.; Mendizabal, F.; Miranda-Rojas, S.; Muñoz-Castro, A. Enhancement of the Catalytic Activity of Fe Phthalocyanine for the Reduction of O2 Anchored to Au (111) via Conjugated Self-Assembled Monolayers of Aromatic Thiols As Compared to Cu Phthalocyanine. *J. Phys. Chem. C* **2012**, *116* (29), 15329−15341.

(30) Yasuda, S.; Kumagai, R.; Nakashima, K.; Murakoshi, K. Electrochemical Potential Stabilization of Reconstructed Au (111) Structure by Monolayer Coverage with Graphene. *J. Phys. Chem. Lett.* **2015**, *6* (17), 3403−3409.

(31) Furche, F.; Ahlrichs, R.; Weis, P.; Jacob, C.; Gilb, S.; Bierweiler, T.; Kappes, M. M. The Structures of Small Gold Cluster Anions as

DOI: 10.1021/acs.jpcc.5b12580
J. Phys. Chem. C 2016, 120, 7358−7364

Determined by a Combination of Ion Mobility Measurements and Density Functional Calculations. *J. Chem. Phys.* **2002**, *117* (15), 6982−6990.
(32) Vargas, A.; Santarossa, G.; Iannuzzi, M.; Baiker, A. Fluxionality of Gold Nanoparticles Investigated by Born-Oppenheimer Molecular Dynamics. *Phys. Rev. B: Condens. Matter Mater. Phys.* **2009**, *80* (19), 1−13.
(33) Deka, A.; Deka, R. C. Structural and Electronic Properties of Stable Aun (n = 2−13) Clusters: A Density Functional Study. *J. Mol. Struct.: THEOCHEM* **2008**, *870* (1−3), 83−93.
(34) Zhao, J.; Yang, J.; Hou, J. Theoretical Study of Small Two-Dimensional Gold Clusters. *Phys. Rev. B: Condens. Matter Mater. Phys.* **2003**, *67* (8), 085404.
(35) Lee, H. M.; Ge, M.; Sahu, B. R.; Tarakeshwar, P.; Kim, K. S. Geometrical and Electronic Structures of Gold, Silver, and Gold−Silver Binary Clusters: Origins of Ductility of Gold and Gold−Silver Alloy Formation. *J. Phys. Chem. B* **2003**, *107* (37), 9994−10005.
(36) Assadollahzadeh, B.; Schwerdtfeger, P. A Systematic Search for Minimum Structures of Small Gold Clusters Aun(n = 2−20) and Their Electronic Properties. *J. Chem. Phys.* **2009**, *131* (6), 064306.
(37) Häkkinen, H.; Yoon, B.; Landman, U.; Li, X.; Zhai, H.-J.; Wang, L.-S. On the Electronic and Atomic Structures of Small Au N - (N = 4−14) Clusters: A Photoelectron Spectroscopy and Density-Functional Study. *J. Phys. Chem. A* **2003**, *107* (32), 6168−6175.
(38) Choi, Y. C.; Kim, W. Y.; Lee, H. M.; Kim, K. S. Neutral and Anionic Gold Decamers: Planar Structure with Unusual Spatial Charge-Spin Separation. *J. Chem. Theory Comput.* **2009**, *5* (5), 1216−1223.
(39) Mukhamedzyanova, D. F.; Ratmanova, N. K.; Pichugina, D. A.; Kuz'menko, N. E. A Structural and Stability Evaluation of Au12 from an Isolated Cluster to the Deposited Material. *J. Phys. Chem. C* **2012**, *116* (21), 11507−11518.
(40) Hakkinen, H. Atomic and Electronic Structure of Gold Clusters: Understanding Flakes, Cages and Superatoms from Simple Concepts. *Chem. Soc. Rev.* **2008**, *37* (9), 1847−1859.
(41) Rieger, R.; Müllen, K. Forever Young: Polycyclic Aromatic Hydrocarbons as Model Cases for Structural and Optical Studies. *J. Phys. Org. Chem.* **2010**, *23* (4), 315−325.
(42) Shekar, S. C.; Swathi, R. S. Cation−π Interactions and Rattling Motion through Two-Dimensional Carbon Networks: Graphene vs Graphynes. *J. Phys. Chem. C* **2015**, *119* (16), 8912−8923.
(43) Umadevi, D.; Sastry, G. N. Molecular and Ionic Interaction with Graphene Nanoflakes: A Computational Investigation of CO2, H2O, Li, Mg, Li+, and Mg2+ Interaction with Polycyclic Aromatic Hydrocarbons. *J. Phys. Chem. C* **2011**, *115* (19), 9656−9667.
(44) Sheng, L.; Ono, Y.; Taketsugu, T. Ab Initio Study of Xe Adsorption on Graphene. *J. Phys. Chem. C* **2010**, *114* (8), 3544−3548.
(45) Cocchi, C.; Prezzi, D.; Ruini, A.; Caldas, M. J.; Molinari, E. Anisotropy and Size Effects on the Optical Spectra of Polycyclic Aromatic Hydrocarbons. *J. Phys. Chem. A* **2014**, *118* (33), 6507−6513.
(46) Faegri Jr, K. *Introduction to Relativistic Quantum Chemistry*; Oxford University Press: New York, 2007.
(47) te Velde, G.; Bickelhaupt, F. M.; Baerends, E. J.; Fonseca Guerra, C.; van Gisbergen, S. J. A.; Snijders, J. G.; Ziegler, T. Chemistry with ADF. *J. Comput. Chem.* **2001**, *22* (9), 931−967.
(48) van Lenthe, E.; Baerends, E. J.; Snijders, J. G. Relativistic Total Energy Using Regular Approximations. *J. Chem. Phys.* **1994**, *101* (11), 9783.
(49) Kenneth, G. Dyall Knut Fægri, J. *Introduction to Relativistic Quantum Chemistry*; Oxford University Press: New York, 2007.
(50) Perdew, J. P.; Burke, K.; Wang, Y. Generalized Gradient Approximation for the Exchange-Correlation Hole of a Many-Electron System. *Phys. Rev. B: Condens. Matter Mater. Phys.* **1996**, *54* (23), 16533−16539.
(51) Perdew, J. P.; Burke, K.; Ernzerhof, M. Generalized Gradient Approximation Made Simple. *Phys. Rev. Lett.* **1996**, *77* (18), 3865−3868.
(52) Swart, M.; Groenhof, A. R.; Ehlers, A. W.; Lammertsma, K. Validation of Exchange−Correlation Functionals for Spin States of Iron Complexes. *J. Phys. Chem. A* **2004**, *108* (25), 5479−5483.
(53) van der Wijst, T.; Guerra, C. F.; Swart, M.; Bickelhaupt, F. M. Performance of Various Density Functionals for the Hydrogen Bonds in DNA Base Pairs. *Chem. Phys. Lett.* **2006**, *426* (4−6), 415−421.
(54) Versluis, L.; Ziegler, T. The Determination of Molecular Structures by Density Functional Theory. The Evaluation of Analytical Energy Gradients by Numerical Integration. *J. Chem. Phys.* **1988**, *88* (1), 322.
(55) Grimme, S. Density Functional Theory with London Dispersion Corrections. *Wiley Interdiscip. Rev. Comput. Mol. Sci.* **2011**, *1* (2), 211−228.
(56) Frisch, M. J.; Trucks, G. W.; Schlegel, H. B.; Scuseria, G. E.; Robb, M. A.; Cheeseman, J. R.; Scalmani, G.; Barone, V.; Mennucci, B.; Petersson, G. A.; et al. *Gaussian 09*.
(57) Andrae, D.; Häußermann, U.; Dolg, M.; Stoll, H.; Preuß, H. Energy-Adjustedab Initio Pseudopotentials for the Second and Third Row Transition Elements. *Theor. Chim. Acta* **1990**, *77* (2), 123−141.
(58) Pyykkö, P. Theoretical Chemistry of Gold. *Angew. Chem., Int. Ed.* **2004**, *43* (34), 4412−4456.
(59) Pyykkö, P.; Runeberg, N.; Mendizabal, F. Theory of the d10−d10 Closed-Shell Attraction: 1. Dimers Near Equilibrium. *Chem. - Eur. J.* **1997**, *3* (9), 1451−1457.
(60) Mendizabal, F. Theoretical Study of the Au−ethylene Interaction. *Int. J. Quantum Chem.* **1999**, *73* (3), 317−324.
(61) Mendizabal, F. Theoretical Study of Gold−Carbonyls Interaction in Au(CO)n (n = 1−3) Complexes. *Organometallics* **2001**, *20* (2), 261−265.
(62) Mendizabal, F.; Salazar, R. Theoretical Study on Electronic Spectra and Interaction in [Au3]-L-[Au3] (L = C6F6,Ag+) Complexes. *J. Mol. Model.* **2013**, *19* (5), 1973−1979.
(63) Bergner, A.; Dolg, M.; Küchle, W.; Stoll, H.; Preuß, H. Ab Initio Energy-Adjusted Pseudopotentials for Elements of Groups 13−17. *Mol. Phys.* **1993**, *80* (6), 1431−1441.
(64) Huzinaga, S. Gaussian-Type Functions for Polyatomic Systems. I. *J. Chem. Phys.* **1965**, *42* (4), 1293.
(65) Pyykko, P.; Runeberg, N.; Mendizabal, F. Theory of the d10-d10 Closed-Shell Attraction: 1. Dimers near Equilibrium. *Chem. - Eur. J.* **1997**, *3* (9), 1451−1457.
(66) Mendizabal, F. Theoretical Study of the Au−ethylene Interaction. *Int. J. Quantum Chem.* **1999**, *73* (3), 317−324.
(67) Mendizabal, F. Theoretical Study of Gold−Carbonyls Interaction in Au(CO) N (N = 1−3) Complexes. *Organometallics* **2001**, *20* (2), 261−265.
(68) Morokuma, K. Molecular Orbital Studies of Hydrogen Bonds. III. C═O···H−O Hydrogen Bond in H_2CO···H_2O and H_2CO···$2H_2O$. *J. Chem. Phys.* **1971**, *55* (3), 1236.
(69) Ziegler, T.; Rauk, A. On the Calculation of Bonding Energies by the Hartree Fock Slater Method. *Theor. Chim. Acta* **1977**, *46* (1), 1−10.
(70) Contreras-García, J.; Johnson, E. R.; Keinan, S.; Chaudret, R.; Piquemal, J.-P.; Beratan, D. N.; Yang, W. NCIPLOT: A Program for Plotting Noncovalent Interaction Regions. *J. Chem. Theory Comput.* **2011**, *7* (3), 625−632.
(71) Saleh, G.; Gatti, C.; Lo Presti, L. Non-Covalent Interaction via the Reduced Density Gradient: Independent Atom Model vs Experimental Multipolar Electron Densities. *Comput. Theor. Chem.* **2012**, *998*, 148−163.
(72) Saleh, G.; Gatti, C.; Lo Presti, L.; Contreras-García, J. Revealing Non-Covalent Interactions in Molecular Crystals through Their Experimental Electron Densities. *Chem. - Eur. J.* **2012**, *18* (48), 15523−15536.

DOI: 10.1021/acs.jpcc.5b12580
J. Phys. Chem. C 2016, 120, 7358−7364